Supporting Information

Highly stable metal-organic framework derived phosphorus doped carbon/Cu_2O structure for efficient photocatalytic phenol degradation and hydrogen production

Amare Aregahegn Dubale [1,2], Ibrahim Nasser Ahmed [1,3], Xia-Hui Chen [4], Cheng Ding [1], Gui-Hua Hou [1], Rong-Feng Guan [1], Xiangming Meng [5], Xiu-Li Yang [1,*] and Ming-Hua Xie [1,*]

[1] Key Laboratory for Advanced Technology in Environmental Protection of Jiangsu Province, Yancheng Institute of Technology, Yancheng 224051, China

[2] Department of Chemistry, College of Natural and Computational Science, Energy and Environment Research Center, Dilla University, Dill 419, Ethiopia

[3] Department of Industrial Chemistry, College of Applied Sciences, Addis Ababa Science and Technology University, Addis Ababa 16417, Ethiopia

[4] School of Electrical, Computer and Energy Engineering, Arizona State University, Tempe 85287, United States

[5] School of Chemistry and Chemical Engineering & Center for Atomic Engineering of Advanced Materials & AnHui Province Key Laboratory of Chemistry for Inorganic/Organic Hybrid Functionalized Materials, Anhui University, Hefei 230601, P.R. China

*Corresponding authors Email: minghxie@163.com, xlychem@126.com

The XRD patterns of the unmodified HKUST-1 and modified HKUST-1 MOF sample at 0.25 wt % triphenylphosphine involvement are shown in Fig. S1. The diffraction patterns of unmodified HKUST-1 are well indexed and the patterns were the same with the simulated XRD pattern The XRD patterns of modified HKUST-1 were also similar with both the synthesized HKUST-1 and the simulated XRD pattern except a new peak emerged at $2\theta = 36.4^{\circ}$ (selected peak) matching well with the diffraction patterns of Cu_2O (JCPDS card number 05-0667). This might be due to partial reduction of Cu^{+2} ions to Cu^{+} ions via TPP. This suggests that the triphenylphosphine incorporation process was successful, and the ligands, triphenylphosphine and trimesic acid, can be involved in coordination reaction with the Cu^{2+} cation.

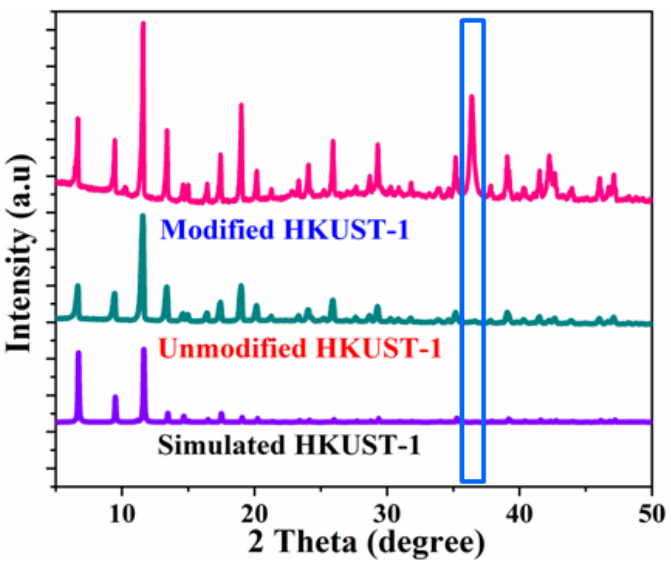

Fig. S1 XRD patterns of modified and unmodified HKUST-1.

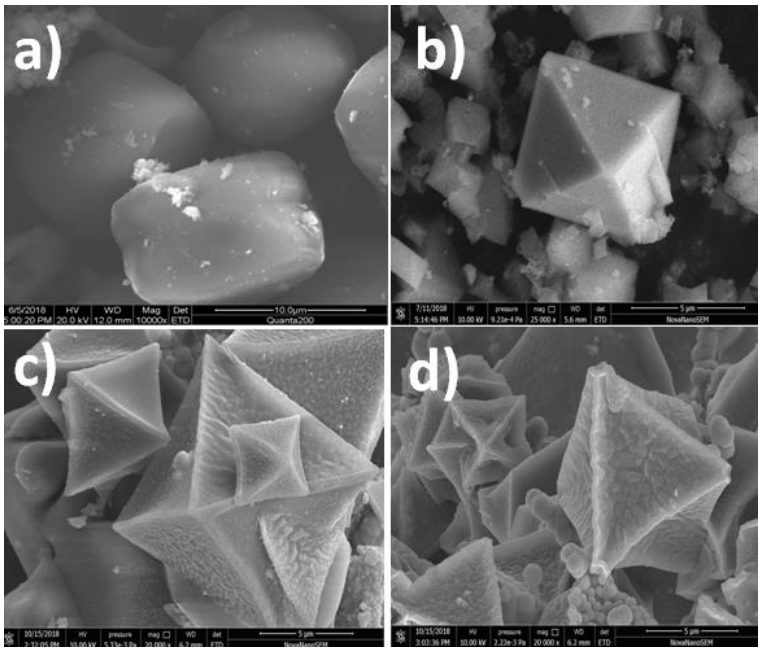

Fig. S2 Scanning electron microscopy (SEM) images of the unmodified HKUST-1 (a) and modified HKUST-1 in presence of 0.25 (b), 0.50 (c) and 0.75 weight ratio of triphenylphosphine.

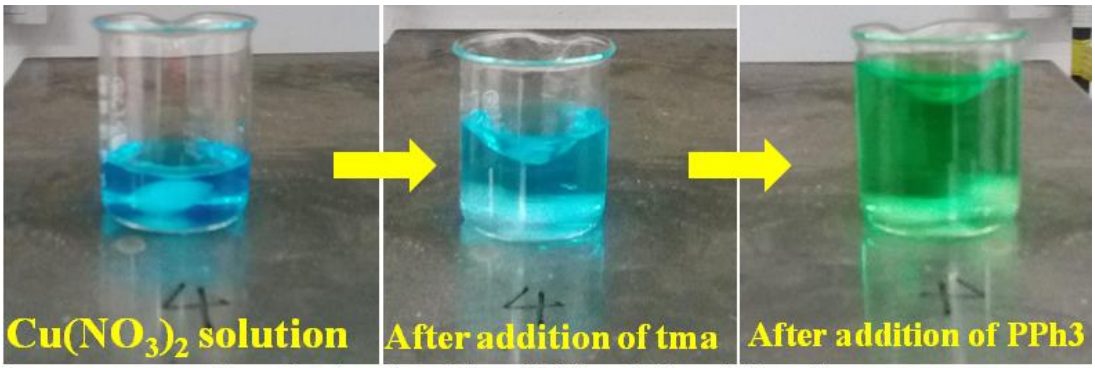

*tma- is trimesic acid and PPh_3- triphenylphosphine

Fig. S3 Digital photographs of solutions during preparation of modified HKUST-1

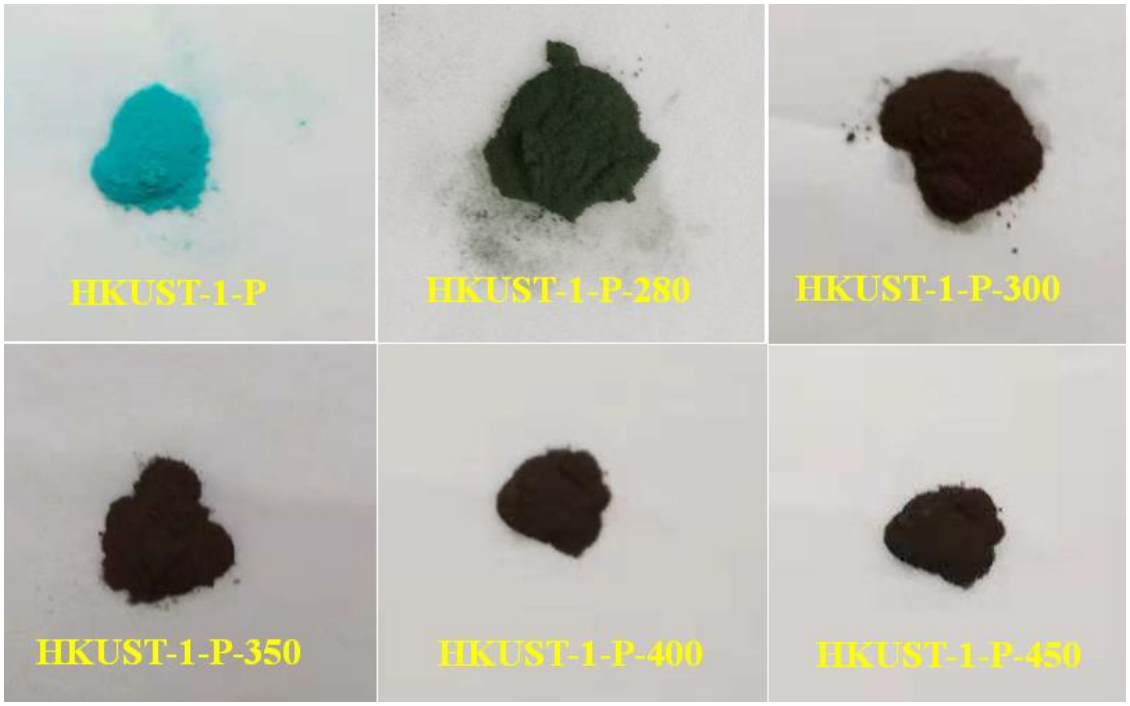

Fig. S4 Digital photographs of different samples

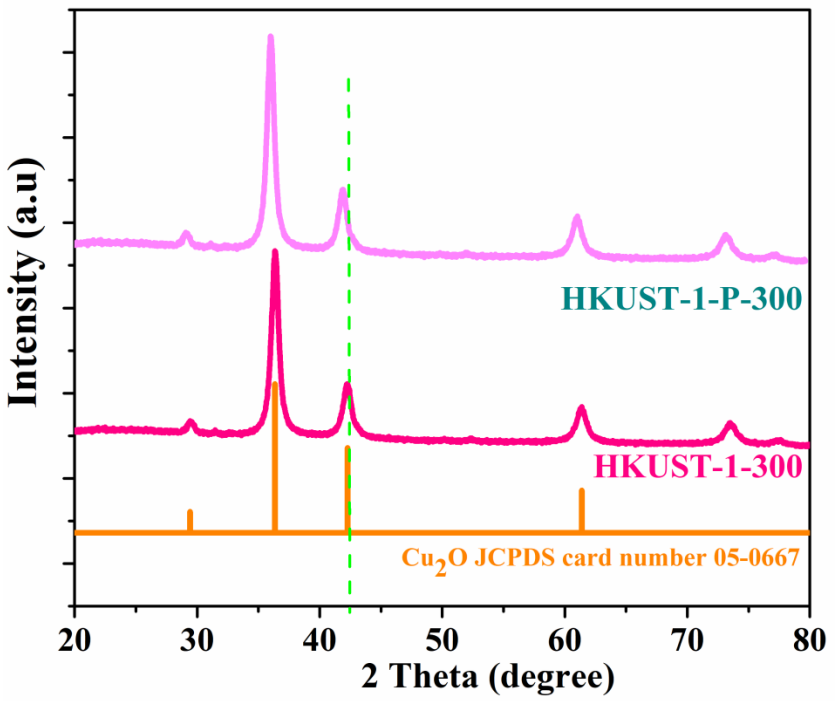

Fig. S5 XRD patterns of HKUST-1-P-300 and HKUST-1-300

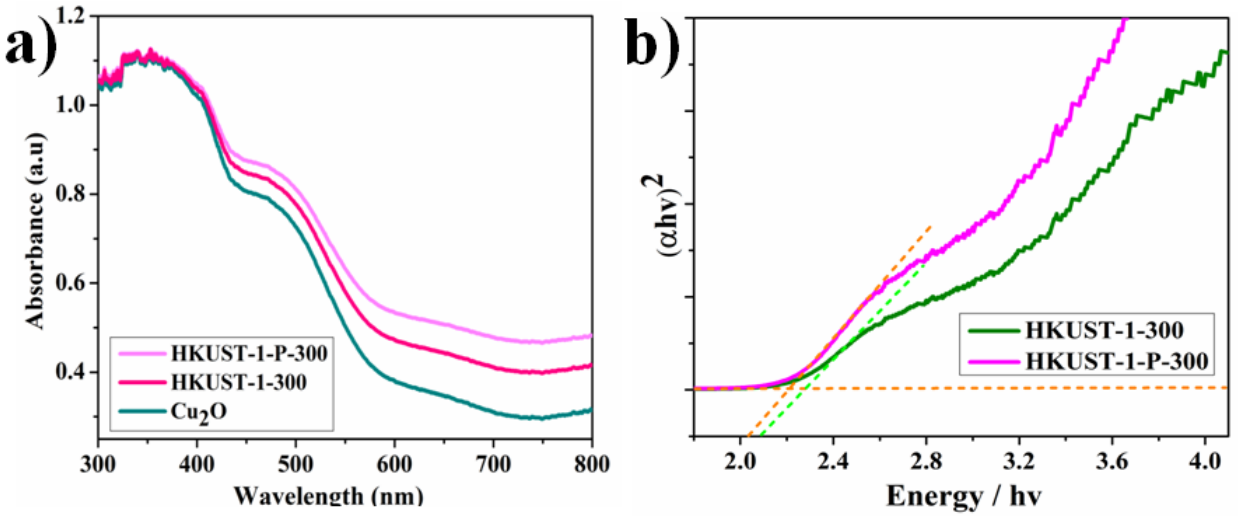

Fig. S6 (a) UV-Vis diffusive absorption spectra of HKUST-1-P-300, HKUST-1-300 and Cu_2O nanoparticles and (b) Tauc plots of HKUST-1-P-300 and HKUST-1-300 samples for band gap estimation.

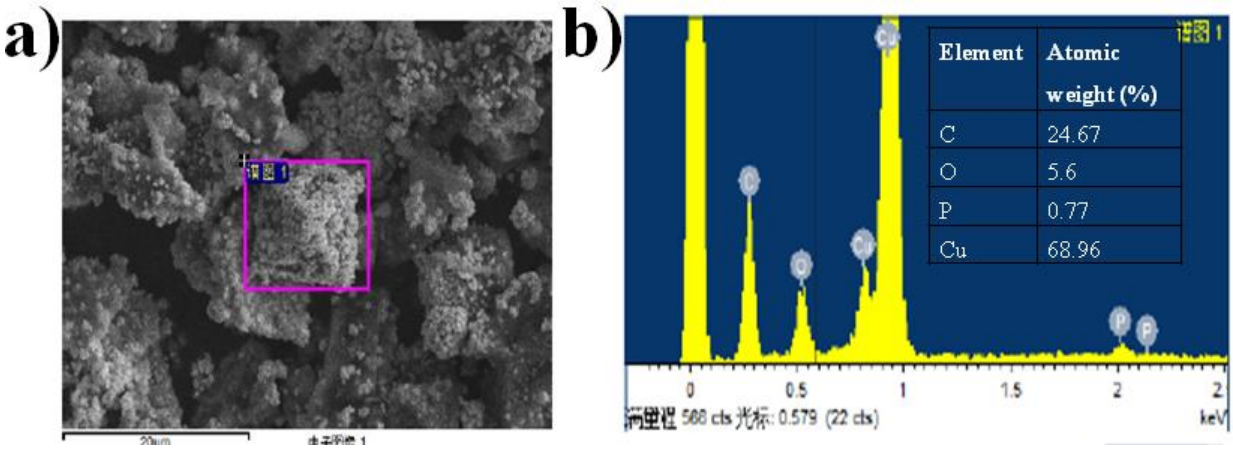

Fig. S7 SEM images (a) and Typical EDX analysis (b) acquired from the HKUST-1-P-300

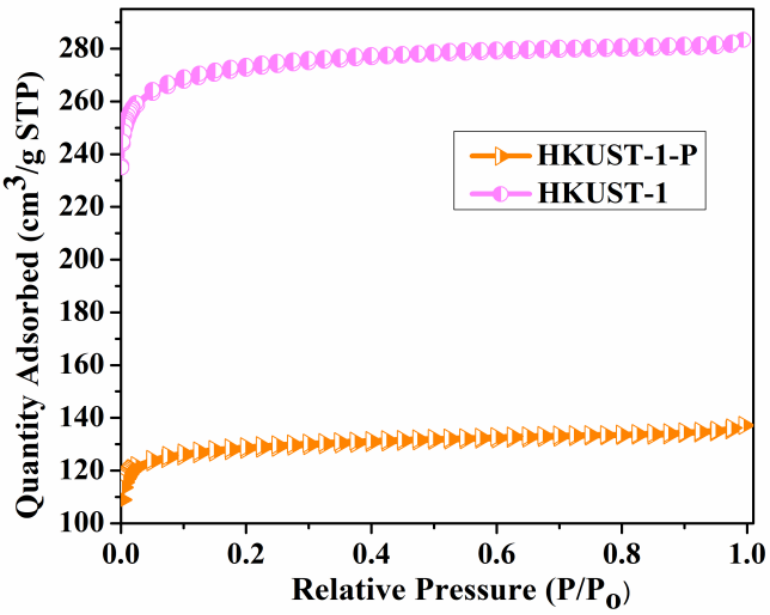

Fig. S8 Nitrogen adsorption and desorption isotherms of HKUST-1 and HKUST-1-P

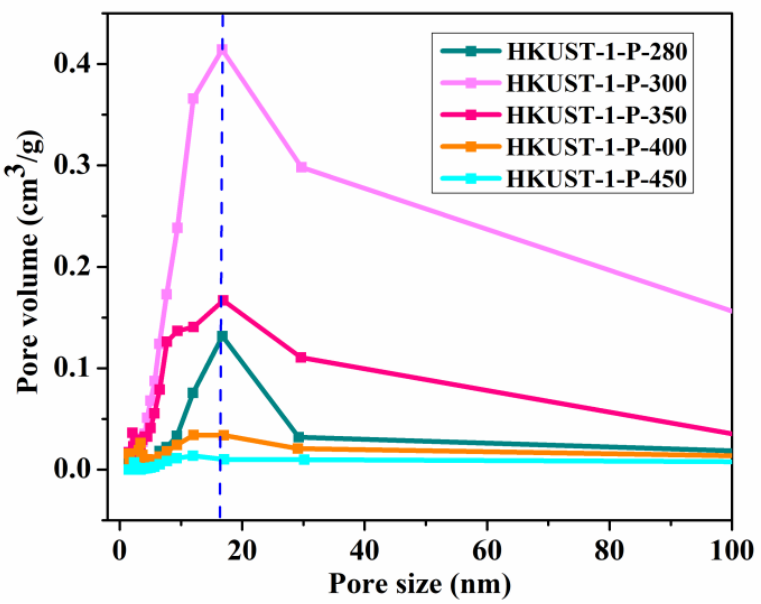

Fig. S9 BJH pore size distribution of different prepared samples

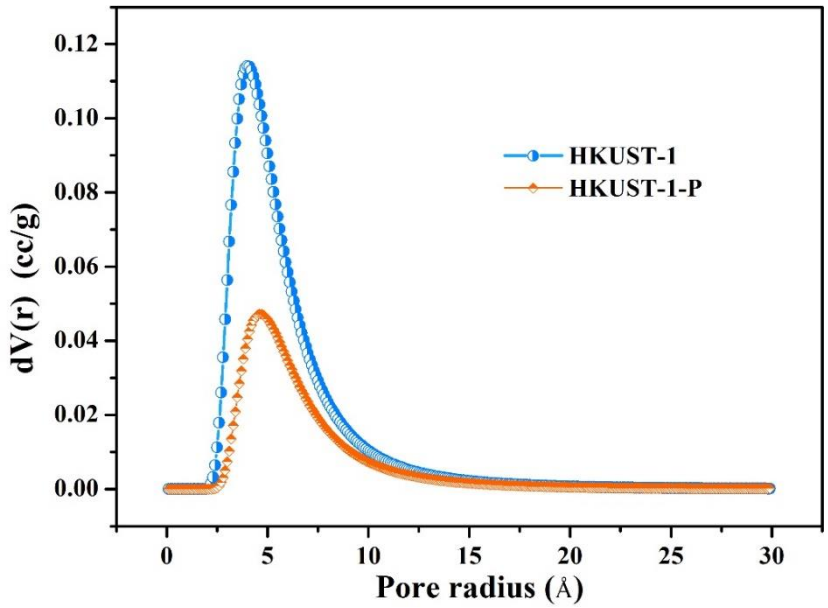

Fig. S10 D-A pore size distribution of MOF precursors.

Table S1 BET information of the prepared samples

Sample	S_{BET} (m^2 g^{-1})	Pore size (nm)	Pore volume (cm^3 g^{-1})
HKUST-1	1103.2	0.41	0.438
HKUST-1-P	517.9	0.46	0.212
HKUST-1-P-280	11.31	16.8	0.059
HKUST-1-P-300	219.2	12.0	0.356
HKUST-1-P-350	28.15	2.1	0.134
HKUST-1-P-400	10.72	1.5	0.034
HKUST-1-P-450	2.73	2.4	0.014

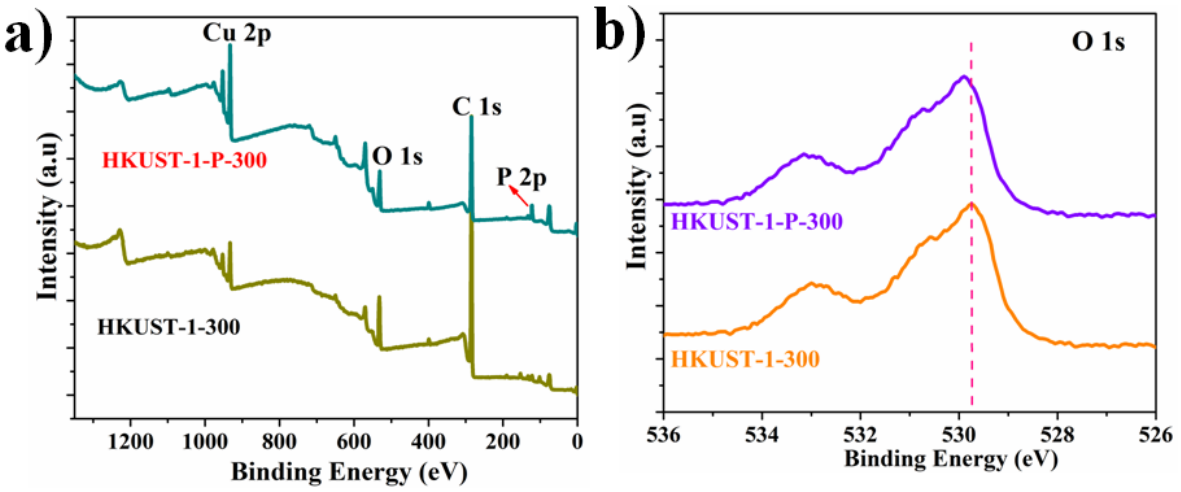

Fig. S11 (a) XPS survey spectra of for HKUST-1-300 and HKUST-1-P-300 and (b) High resolution XPS spectra of O 1s for HKUST-1-300 and HKUST-1-P-300 samples.

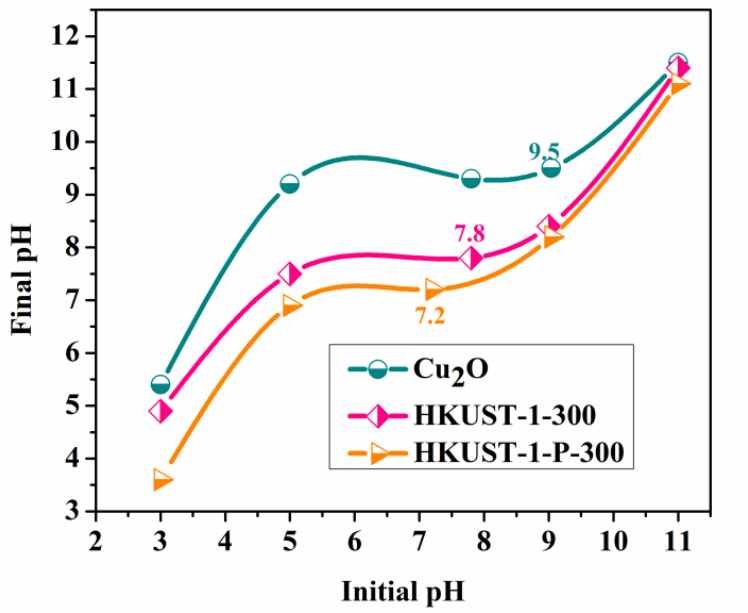

Fig. S12 pH_{pzc} analysis of HKUST-1-P-300, HKUST-1-300 and Cu_2O.

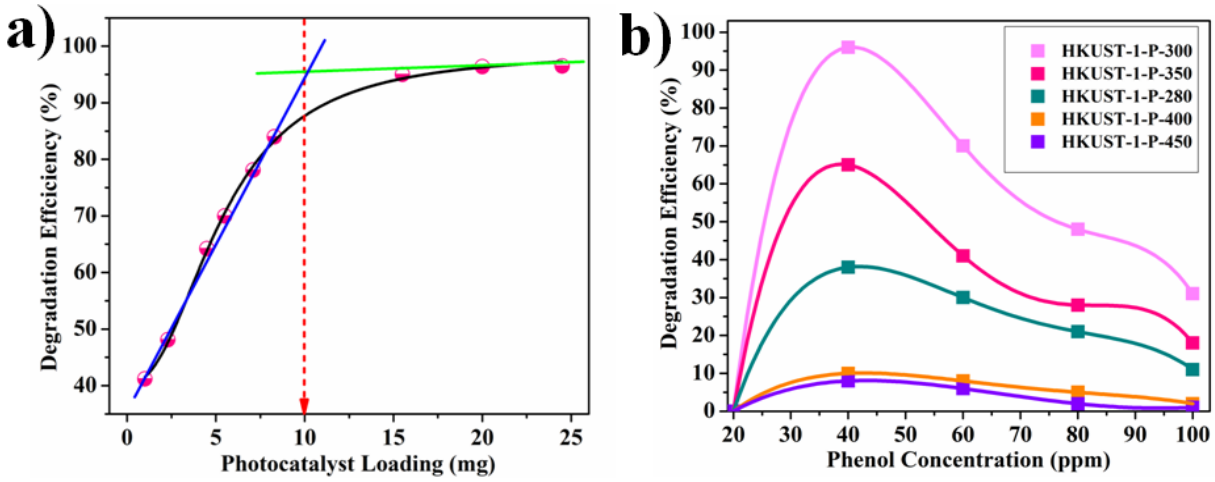

Fig. S13 (a) Degradation efficiency of phenol vs. photocatalyst loading and (b) effect of phenol initial concentration in presence of HKUST-1-P-280, HKUST-1-P-300, HKUST-1-P-350, HKUST-1-P-400 and HKUST-1-P-450 photocatalyst (10 mg photocatalyst dose and at pH 6.8) under visible light irradiation for 2 h.

Table S2 Effect of phenol initial concentration in presence of HKUST-1-P-280, HKUST-1-P-300, HKUST-1-P-350, HKUST-1-P-400 and HKUST-1-P-450 photocatalyst (10 mg photocatalyst dose and at pH 6.8 under visible light irradiation for 2 h.

Initial phenol concentration (ppm)	Degradation efficiency (%) of phenol by different photocatalyst				
	HKUST-1-P-280	HKUST-1-P-300	HKUST-1-P-350	HKUST-1-P-400	HKUST-1-P-450
20	-	-	-	-	-
40	38	96	65	10	8
60	30	70	41	8	6
80	21	48	28	5	2
100	11	31	18	2	1

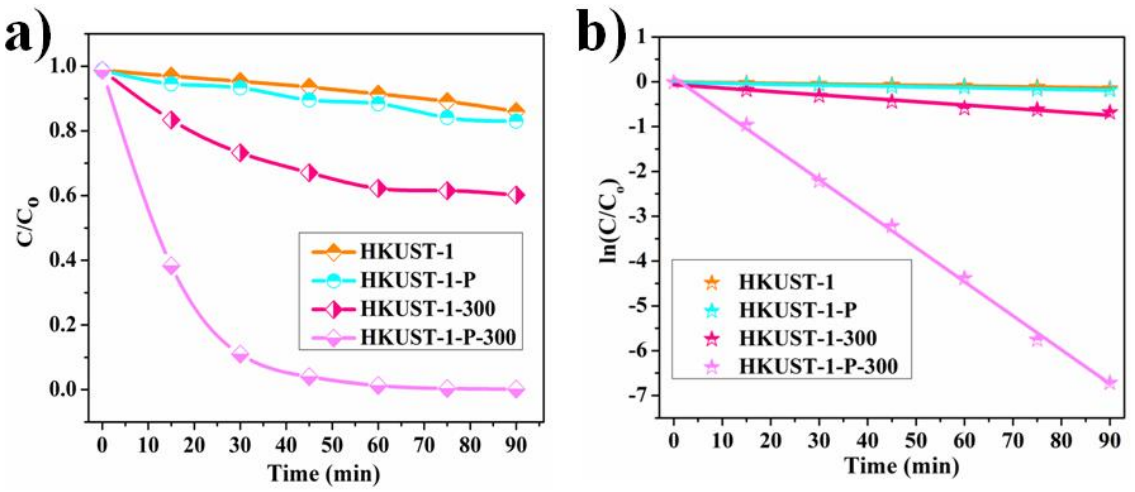

Fig. S14 (a) Degradation efficiency of phenol and (b) corresponding pseudo-first-order kinetic curves of modified and unmodified sample (10 mg catalyst dosage, 40 ppm of phenol solution and at pH 7) under visible light irradiation for 1.5 h.

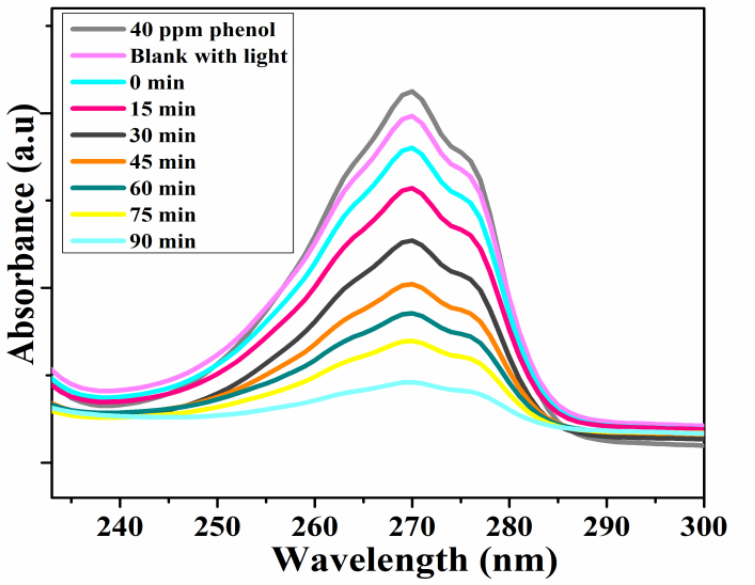

Fig. S15 UV-Vis spectral changes of the degradation of phenol using HKUST-1-P-300

Table S3 Summary of the phenol photo degradation catalyzed by different catalyst.

Sample	Apparent rate constant (min^{-1})	Degradation efficiency (%)	Moles of phenol degraded	TON (60 min)	TOF (min^{-1})
HKUST-1-P	0.0018	11.6	4.93×10^{-3}	1389	23.2
HKUST-1-P-280	0.0074	49.6	2.11×10^{-2}	5944	99.1
HKUST-1-P-300	0.075	99.4	4.25×10^{-2}	11887	198.1
HKUST-1-P-350	0.013	72.1	3.06×10^{-2}	8620	143.7
HKUST-1-P-400	0.0019	18.9	8.03×10^{-3}	2262	37.7
HKUST-1-P-450	0.0014	13.9	5.91×10^{-3}	1665	27.8

The turnover number and the corresponding turnover frequency for phenol degradation were calculated using equation (1) and (2) as follows:

$$TON = \frac{the\ moles\ of\ phenol\ degraded}{the\ moles\ of\ phosphorus\ loaded\ to\ the\ photocatalyst} \qquad equation\ (1)$$

$$TOF = \frac{TON}{time\ (\mathrm{min})} \qquad equation\ (2)$$

For instance, the corresponding TON and TOF of phenol degradation using HKUST-P-300 was calculated to be:

$$TON = \frac{4.25 \times 10^{-2}}{0.01 \times 1.1\% \times \frac{1}{30.974}} = 11887$$

$$TOF = \frac{11887}{60\ min} = 198.1\ min^{-1}$$

Table S4 Photodegradation of phenol using different photocatalyst

Photocatalyst	Initial phenol concentration (ppm)	Time (min)	pH	Irradiation	Degradation (%)	Ref.
n-TiO_2 (77 nm)	37.6	180	7	direct sunlight	87.3	1
n-TiO_2 (77 nm)	37.6	180	7	direct sunlight	95.2	1
Eosin Y-TiO_2/Pt	40	90	7	visible light	93	2
ZnO nanorods	10	150	-	visible light	50	3
TMU-5(Cd 30%)	25	120	6.8	visible light	78	4
V-doped α-MnO_2	100	720	6	UV light	76.8	5
$Fe[HO_3PCH(OH)COO]\cdot 2H_2O$	50	80	7.9	UV light	90	6
$CuO{-}Co_3O_4$	~20	30	-	UV light	~90	7
α-Fe_2O_3/RGO	10	120	-	visible light	67	8

$BiOCl-TiO_2$	50	360	-	visible light	40	9
BiOI-loaded ZnO	25	120		UV light	99.9	10
Ag_3PO_4-$BiOCl_{0.75}Br_{0.25}$ (1:5)	25	75	-	visible light	97.9	11
N-doped TiO_2	50	540		visible light	99.2	12
M-ZnO	25	200		visible light	61.8	13
HKUST-1-P-300 (P-doped carbon/Cu_2O)	**40**	**60**	**7**	**visible light**	**99.4**	**This study**

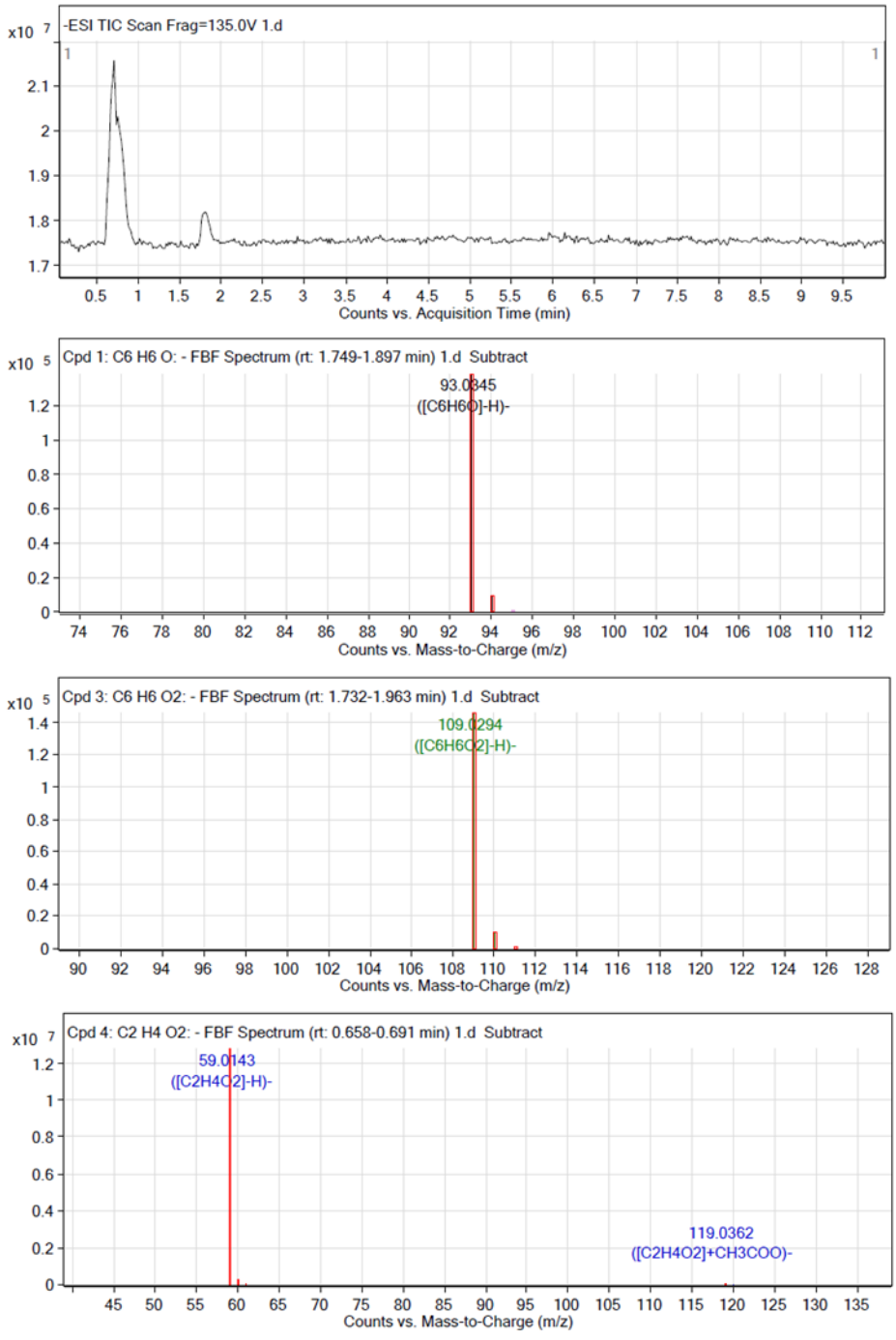

Fig. S16 HPLC-MS spectrum and MS spectra of phenol photo degradation catalyzed by HKUST-1-P-300: irradiated for 15 minutes.

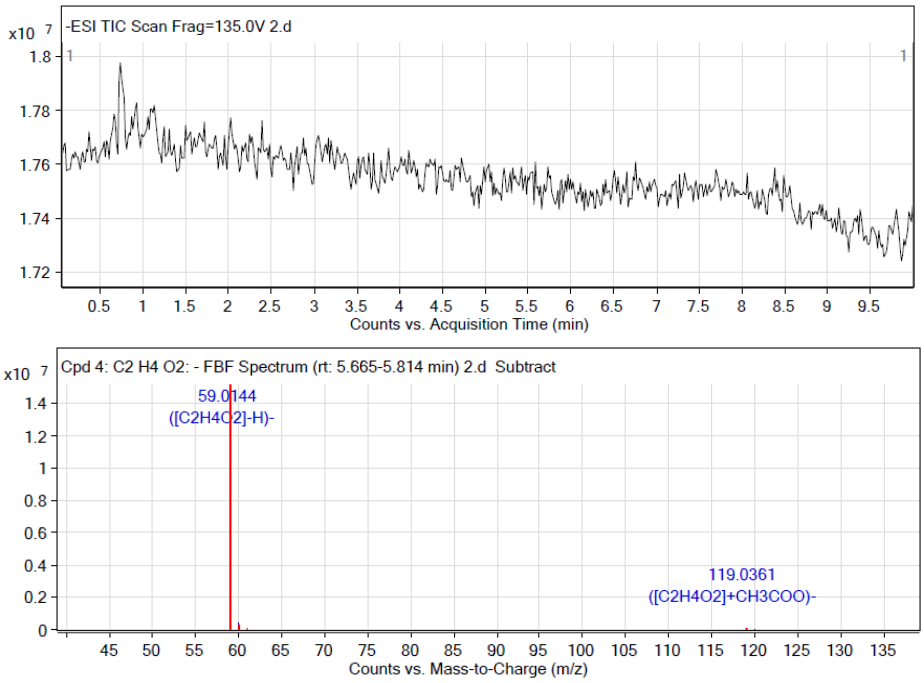

Fig. S17 HPLC-MS spectrum and MS spectrum of phenol photo degradation catalyzed by HKUST-1-P-300: irradiated for 30 minutes.

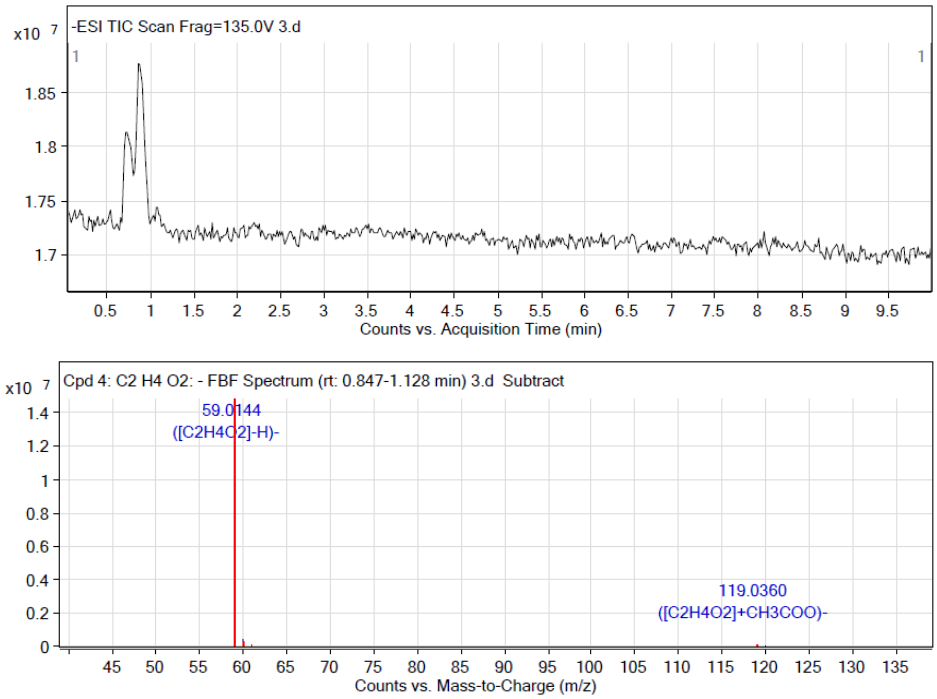

Fig. S18 HPLC-MS spectrum and MS spectrum of phenol photo degradation catalyzed by HKUST-1-P-300: irradiated for 45 minutes

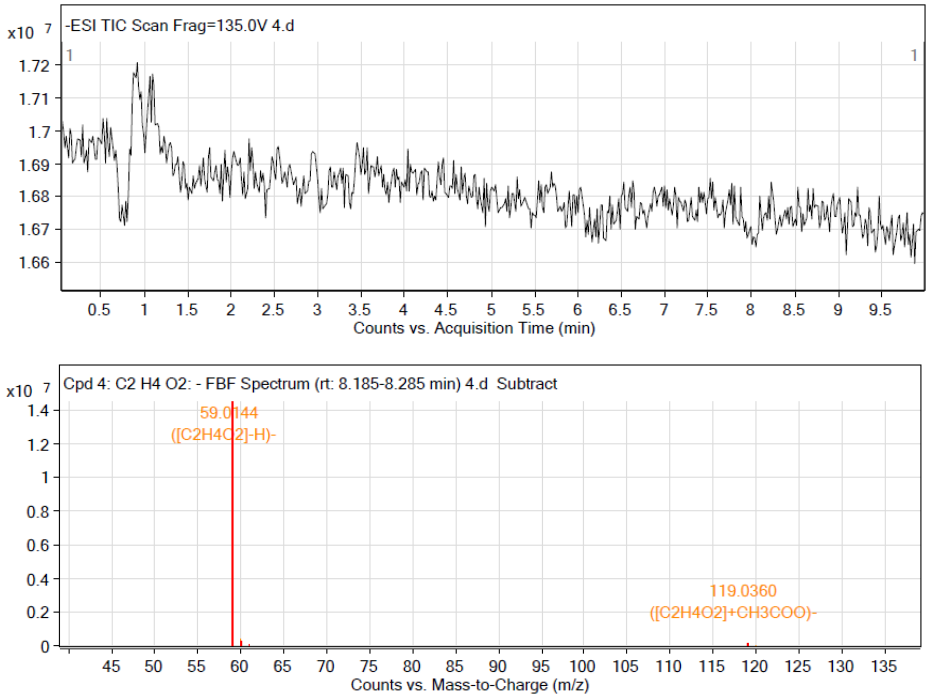

Fig. S19 HPLC-MS spectrum and MS spectrum of phenol photo degradation catalyzed by HKUST-1-P-300: irradiated for 60 minutes.

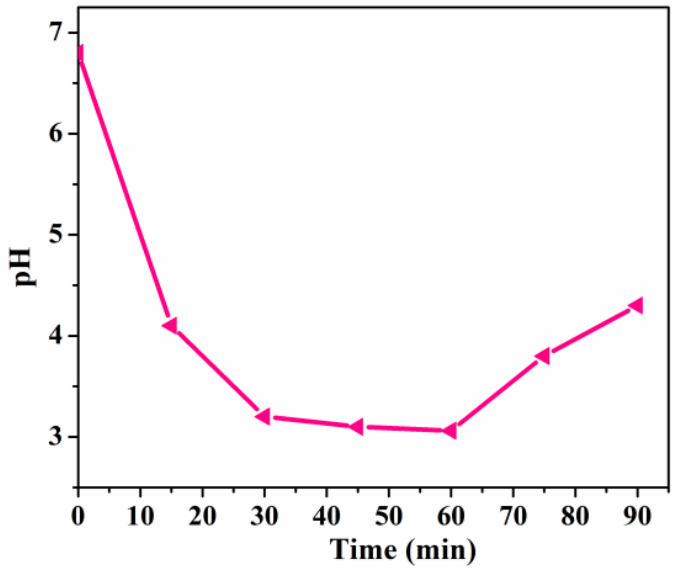

Fig. S20 pH changes in the phenol solution vs. photocatalysis time using HKUST-1-P-300.

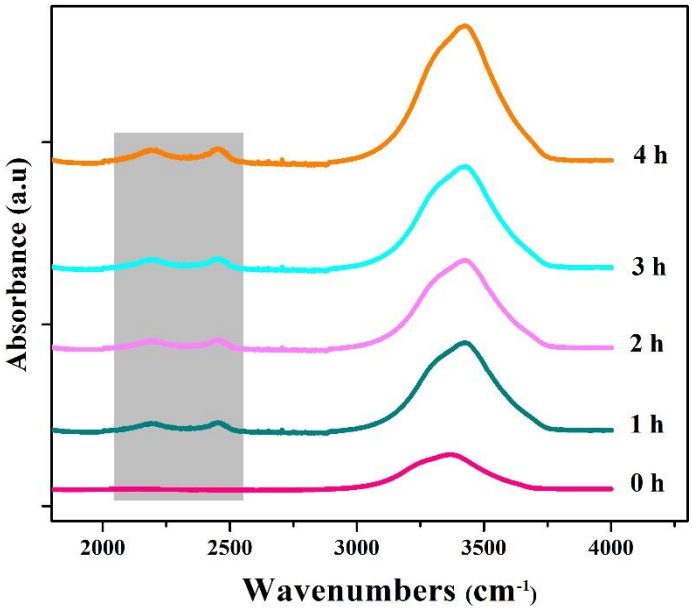

Fig. S21 FTIR spectra for evolution of CO_2 as an indication of complete mineralization of phenol molecules. Reaction time was extended to 4h to give a clear observation of the characteristic absorption peak (gray zone) of CO_2.

Table S5 Theoretical mass balance between MeOH and thus generated CO_2 & H_2 during photochemical H_2 production catalyzed by HKUST-1-P-300. UV absorption at 190 nm was used to calculate the MeOH concentration value (g mL^{-1}).

$CH_3OH + H_2O \longrightarrow CO_2 + 3H_2$			
Time (h)	Methanol concentration	Theoretical CO_2 conc.	Theoretical H_2 conc.
0	0.155	0	0
1	0.140	0.0148	0.0443
2	0.131	0.0238	0.0714
3	0.130	0.0249	0.0749
4	0.127	0.0281	0.0842

Table S6 Change of gas phase CO_2 & H_2 concentration in the reactor during photochemical H_2 production catalyzed by HKUST-1-P-300. GC-TCD technology was used to determine the data.

Time (h)	CO_2 composition (%)	H_2 composition (%)
0	0	0
1	0.28	99.72
2	0.48	99.52
3	0.52	99.48
4	0.60	99.4

Table S7 Comparison of hydrogen production via photochemical water splitting using bare or modified Cu_2O based photocatalyst.

Photocatalyst	Co-catalyst	Sacrificial agent	H_2 evolution rate ($\mu mol\ h^{-1}$)	Ref.
Cu_2O/ MoS_2	MoS_2	Methanol	45.0	14
[a]rGO/Cu_2O	Pt	Methanol	2.645	15
Zn-Doped Cu_2O	Pt	Glucose	38.17	16
Cu_2O/rGO	-	TEOA	45.3	17
[b]NGQDs-Cu_2O	Pt	Methyl alcohol	2.26	18
Cu_2O	-	-	2	19
Cu–Cu_2O–graphene	Pt	Methanol	1.62	20
HKUST-1-P-300	**-**	**Methanol**	**151**	**This work**

[a]rGO- reduced graphene oxide; [b]NGQDs- nitrogen doped graphene quantum dots;

Fig. S22 Digital photo of the reaction mixture during irradiation

The external quantum efficiency (EQE) was measured under the same photocatalytic reaction condition as described before except that irradiation of light from Xenon lamp was carried out at different wavelength (425, 440, 480, 520 and 600 nm) by using a monochromator (monochromator: omno151). The light intensity was obtained with an optical power meter (FZ-400, HSX-F300 Beijing), and the number of incident photons and quantum efficiency were obtained by equation (3) and equation (4), respectively. The amounts of H_2 molecules generated in 3 h using HKUST-1-P-300 are used for calculation of external quantum efficiency.

$$N = \frac{E\lambda}{hc} \qquad equation\ (3)$$

$$EQE = \frac{2 \times the\ number\ of\ evolved\ H_2\ molecules}{the\ number\ of\ incident\ photons} \times 100\% \quad equation\ (4)$$

For instance, the corresponding number of incident photons (N) and external quantum efficiency (EQE) at 425 nm was calculated to be 4.85x10^{19} and 48.6%, respectively. That is:

$$N = \frac{E\lambda}{hc} = \frac{2.1 \times 10^{-3} \times 3 \times 3600 \times 425 \times 10^{-9}}{6.626 \times 10^{-34} \times 3 \times 10^{8}} = 4.85 \times 10^{19}$$

$$EQE = \frac{2 \times 6.02 \times 10^{23} \times 19.57 \times 10^{-6}}{4.85 \times 10^{19}} = 48.6\%$$

Table S8 The calculated External Quantum Efficiency (EQE) at different wavelength

Sample	Wavelength (nm)	H_2 evolved (μmol)	Light intensity (mW)	No of incident photon (N)	EQE (%)
HKUST-1-P-300	λ=425	19.57	2.1	4.85×10^{19}	48.6
	λ=440	15.32	2.7	6.45×10^{19}	28.2
	λ=480	9.28	5.1	1.33×10^{20}	8.4
	λ=520	2.23	5.5	1.49×10^{20}	1.8
	λ=600	0.216	4.1	1.30×10^{20}	0.2
HKUST-1-P-280	λ=425	1.25	2.1	4.85×10^{19}	3.1
HKUST-1-P-350	λ=425	3.30	2.1	4.85×10^{19}	8.2
HKUST-1-P-400	λ=425	0.483	2.1	4.85×10^{19}	1.2
HKUST-1-P-450	λ=425	0.384	2.1	4.85×10^{19}	0.84
HKUST-1-P	λ=425	0.0004	2.1	4.85×10^{19}	0.001

The turnover number and the corresponding turnover frequency for hydrogen evolution were calculated by using equation (5) below and equation (4) above, respectively. The amount of evolved H_2 using HKUST-1-P-300 photocatalyst is ~1208 μmol in 8 h.

$$TON = \frac{the\ moles\ of\ evolved\ H_2}{the\ moles\ of\ phosphorus\ loaded\ to\ the\ photocatalyst} \quad equation\ (5)$$

$$TON = \frac{1208 \times 10^{-6}}{0.01 \times 1.1\% \times \frac{1}{30.974}} = 340.2$$

$$TOF = \frac{340.2}{8\ h} = 42.5\ h^{-1}$$

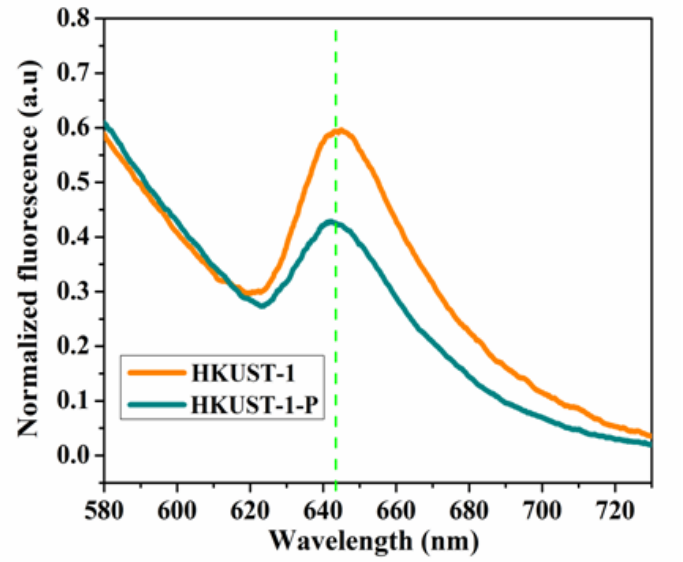

Fig. S23 Photoluminescence spectra of HKUST-1 and unmodified HKUST-1-P

Theoretical studies of P-doping

All calculations were performed using the Perdew-Burke-Ernzerhof (GGA-PBE)[21] exchange-correlation functional implemented in the plane-wave based Vienna ab initio simulation package (VASP)[22-24], the projector augmented wave (PAW) method[25, 26] with a frozen-core approximation was used to describe the ion-electron interactions. A cutoff energy of 400 eV and the conjugate-gradient algorithm were used in the calculations. Brillouin-zone integrations were done with Monkhorst Pack[27] grids using a generalized Gaussian smearing width of 0.1 eV.[28] Density of states (DOS) was calculated with (5×5×1) *k*-points grids for Cu_2O and P-doped Cu_2O. The substrate is modeled with four-layer slab of 4×4 surface unit, subjected to three-dimensional periodic boundary conditions. The slabs were separated by vacuums of 15 Å. The bottom two atomic layers were fixed at theoretical equilibrium bulk positions of Cu and O, while all the other atoms were allowed to relax. The band gap values calculated from DFT results are usually much smaller than that of measured values, however it is still could be used for mutual comparison to get the regularity of materials because they were studied under the same standard.[29]

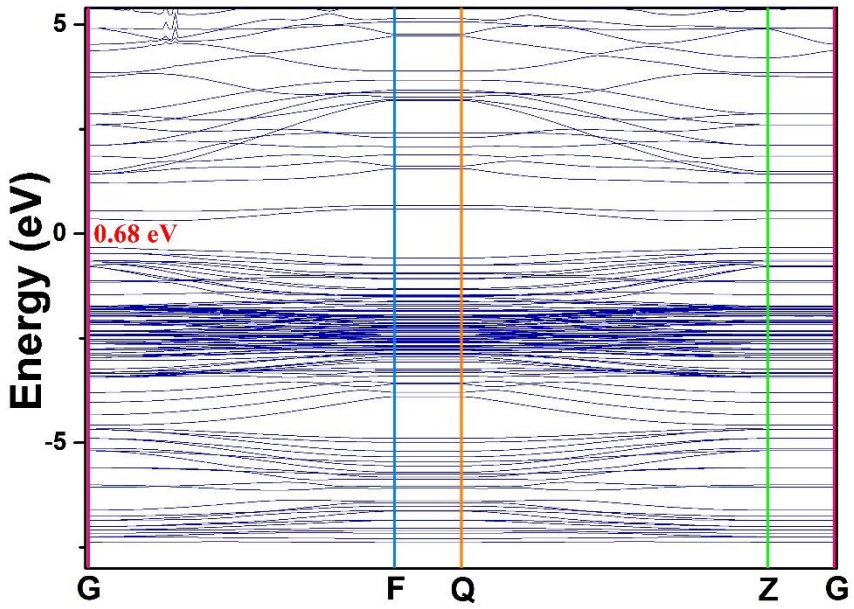

Fig. S24 Electronic band structure of Cu_2O (1, 1, 1).

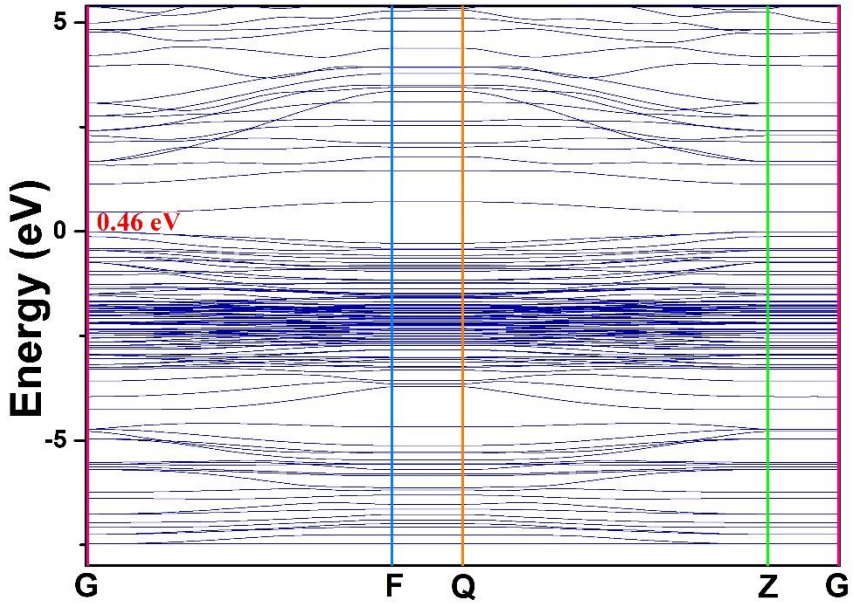

Fig. S25 Electronic band structure of P-Cu_2O (1, 1, 1).

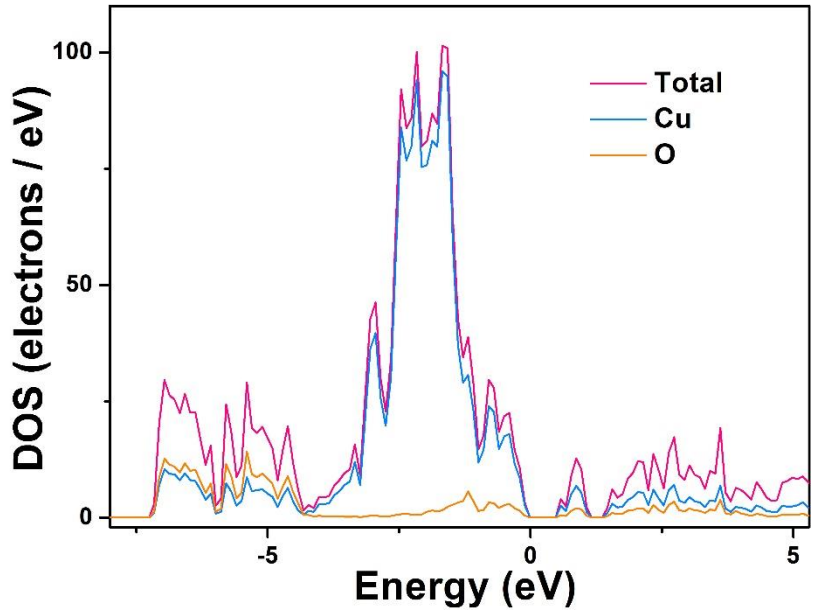

Fig. S26 PDOS and TDOS of Cu_2O (1, 1, 1).

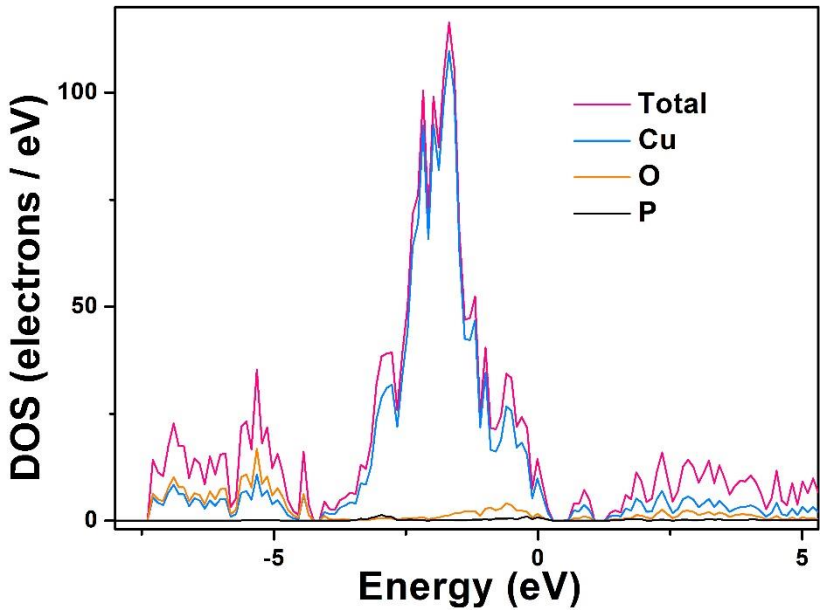

Fig. S27 PDOS and TDOS of P-Cu_2O (1, 1, 1).

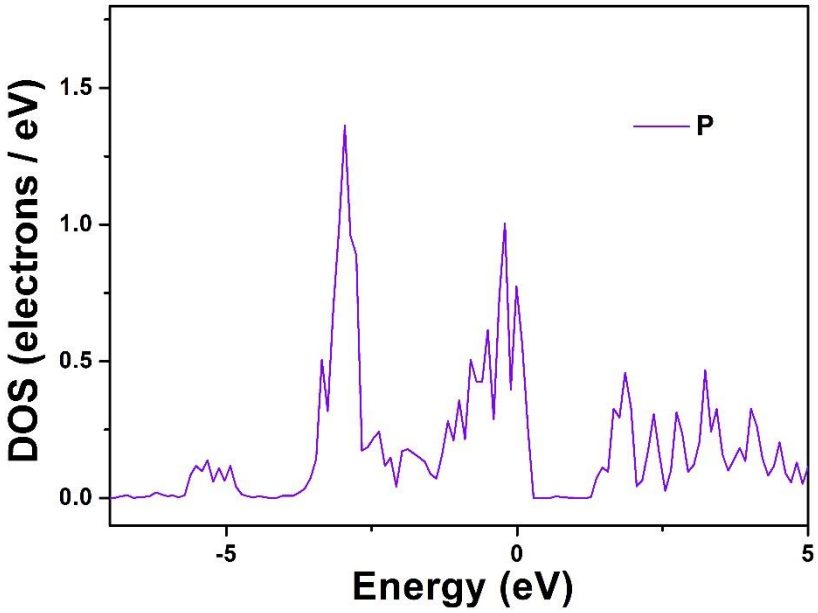

Fig. S28 PDOS of phosphorus in P-Cu_2O (1, 1, 1).

References:

1. A. M. Asiri, M. S. Al-Amoudi, T. A. Al-Talhi and A. D. Al-Talhi, Photodegradation of Rhodamine 6G and phenol red by nanosized TiO_2 under solar irradiation, *J. Saudi Chem. Soc.*, 2011, **15**, 121–128.
2. P. Chowdhury, J. Moreira, H. Gomaa and A. K. Ray, Visible-solar-light-driven photocatalytic degradation of phenol with dye-sensitized TiO_2: Parametric and kinetic study, *Ind. Eng. Chem. Res.*, 2012, **51**, 4523–4532.
3. J. Al-Sabahi, T. Bora, M. Al-Abri and J. Dutta, Controlled defects of zinc oxide nanorods for efficient visible light photocatalytic degradation of phenol, *Materials.*, 2016, **9**. 238: doi:10.3390/ma9040238.
4. M. Y. Masoomi, M. Bagheri, A. Morsali and P. C. Junk, High photodegradation efficiency of phenol by mixed-metal–organic frameworks, *Inorg. Chem. Front.*, 2016, **3**, 944–951
5. S. Chen, S. Zhang, T. Wang, Z. Lei, M. Zhu, X. Dai, F. Liu, J. Li and H. Yin, Structure and properties of vanadium-doped α-MnO_2 and enhanced Pb^{2+} adsorption phenol/photocatalytic degradation, *Mater. Chem. Phys.*, 2018, **208**, 258–267.

6. M. Bazaga-Garcia, A. Cabeza, P. Olivera-Pastor, I. Santacruz, R. M. P. Colodrero and M. A. G. Aranda, Photodegradation of phenol over a hybrid organo-inorganic material: Iron(II) hydroxyphosphonoacetate, *J. Phys. Chem. C*, 2012, **116**, 14526–14533.
7. W. Shi and N. Chopra, Controlled fabrication of photoactive copper oxide−cobalt oxide nanowire heterostructures for efficient phenol photodegradation, *ACS Appl. Mater. Interfaces*, 2012, **4**, 5590–5607.
8. G. K. Pradhan, D. K. Padhi and K. M. Parida, Fabrication of α-Fe_2O_3 nanorod/RGO composite: a novel hybrid photocatalyst for phenol degradation, *ACS Appl. Mater. Interfaces*, 2013, **5**, 9101–9110.
9. D. Sánchez-Rodríguez, M. G. Méndez Medrano, H. Remita and V. Escobar-Barrios, Photocatalytic properties of BiOCl-TiO_2 composites for phenol photodegradation, *J. Environ. Chem. Eng.*, 2018, **6**, 1601–1612.
10. J. Jiang, H. Wang, X. Chen, S. Li, T. Xie, D. Wang and Y. Lin, Enhanced photocatalytic degradation of phenol and photogenerated charges transfer property over BiOI-loaded ZnO composites, *J. Colloid Interface Sci.*, 2017, **494**, 130–138.
11. Y. L. Qi, G. Han and X. C. Song, Enhanced photocatalytic degradation of phenol over Ag_3PO_4-$BiOCl_{1-x}Br_x$ composites, *Mater. Res. Bull.*, 2018, **102**, 16–23.
12. M. A. Mohamed,, W.N.W. Salleh, J. Jaafar, A.F. Ismail and N. A. M. Nor, Photodegradation of phenol by N-Doped TiO_2 anatase/rutile nanorods assembled microsphere under UV and visible light irradiation, *Mater. Chem. Phys.*, 2015, 162, 113–123
13. Z.-J Wu, W. Huang, K.-K Cui, Z.-F Gao and P. Wang, Sustainable synthesis of metals-doped ZnO nanoparticles from zinc-bearing dust for photodegradation of phenol, *J. Hazard. Mater.*, 2014, 278, 91–99
14. Y.-F. Zhao, Z.-Y. Yang, Y.-X. Zhang, L. Jing, X. Guo, Z. Ke, P. Hu, G. Wang, Y.-M. Yan and K.-N. Sun, Cu_2O decorated with cocatalyst MoS_2 for solar hydrogen production with enhanced efficiency under visible light, *J. Phys. Chem. C.*, 2014, **118**, 14238–14245.
15. P. D. Tran, S. K. Batabyal, S. S. Pramana, J. Barber, L. H. Wong and S. C. Loo, A cuprous oxide-reduced graphene oxide (Cu_2O-rGO) composite photocatalyst for hydrogen generation: employing rGO as an electron acceptor to enhance the photocatalytic activity and stability of Cu_2O, *Nanoscale*, 2012, **4**, 3875–3878.

16. L. Zhang, D. Jing, L. Guo, and X. Yao, In Situ photochemical synthesis of Zn-Doped Cu_2O hollow microcubes for high efficient photocatalytic H_2 production, *ACS Sustainable Chem.*, Eng. 2014, **2**, 1446−1452.
17. H. Xu, X. Li, S.-Z Kang, L. Qin, G. Li and J. Mu, Noble metal-free cuprous oxide/reduced grapheme oxide for enhanced photocatalytic hydrogen evolution from water reduction, *Int. J. Hydrogen Energy.*, 2014, **39**, 11578–11582.
18. Y. Wu, M. Yan, J. Gao, P. Lv, X. Liu, C. Li and Y. Yan, Fabrication of nitrogen-doped graphene quantum dots-Cu_2O catalysts for enhanced photocatalytic hydrogen evolution, *Nano,* 2018, **8**, 1850099: doi: 10.1142/S1793292018500996.
19. M. Hara, T. Kondo, M. Komoda, S. Ikeda, K. Shinohara, A. Tanaka, J. N. Kondo and K. Domen, Cu_2O as a photocatalyst for overall water splitting under visible light irradiation, *Chem. Commun.*, 1998, **0**, 357–358
20. D. Zhang, D. Wei, Z. Cui, S. Wang, S. Yang, M. Cao and C. Hu, Improving water splitting performance of Cu_2O through a synergistic ‘‘two-way transfer’’ process of Cu and graphene, *Phys. Chem. Chem. Phys.*, 2014, **16**, 25531–25536.
21. P. Perdew, J. A. Chevary, S. H. Vosko, K. A. Jackson, M. R. Pederson, D. J. Singh and C. Fiolhais, *Phys. Rev. B:Condens. Matter Mater. Phys.*, 1992, **46**, 6671–6687.
22. G. Kresse and J. Furthmüller, *Phys. Rev. B*, 1996, **54**, 11169.
23. G. Kresse and J. Furthmüller, *Comput. Mater. Sci.*, 1996, **6**, 15.
24. G. Kresse and J. Hafner, *Phys. Rev. B*, 1993, **47**, 558.
25. J. P. Perdew, J. A. Chevary, S. H. Vosko, K. A. Jackson, M. R. Pederson, D. J. Singh, and C. Fiolhais, *Phys. Rev. B*, 1992, **46**, 6671.
26. J. A. White and D. M. Bird, *Phys. Rev. B*, 1994, **50**, 4954.
27. H. J. Monkhorst and J. D. Pack, *Phys. Rev. B*, 1976, **13**, 5188.
28. M. Methfessel and A. T. Paxton, *Phys. Rev. B*, 1989, **40**, 3616.
29. W. Yu, D. Xu and T. Peng, *J. Mater. Chem. A*, 2015, **3**, 19936